

# Elevated pressure low-temperature oxidation of linear five-heavy-atom fuels: diethyl ether, *n*-pentane, and their mixture

Luc-Sy Tran<sup>1,2,3</sup>, Yuyang Li<sup>4</sup>, Meirong Zeng<sup>4</sup>, Julia Pieper<sup>3</sup>,  
Fei Qi<sup>4</sup>, Frédérique Battin-Leclerc<sup>2</sup>, Katharina Kohse-Höinghaus<sup>3</sup>, Olivier Herbinet<sup>2</sup>

<sup>1</sup> Physicochimie des Processus de Combustion et de l'Atmosphère (PC2A), CNRS UMR 8522, Université de Lille, F-59000 Lille, France

<sup>2</sup> Laboratoire Réactions et Génie des Procédés (LRGP), CNRS, Université de Lorraine, ENSIC, 1, rue Grandville, BP 20451, 54001 Nancy Cedex, France

<sup>3</sup> Department of Chemistry, Bielefeld University, Universitätsstraße 25, D-33615 Bielefeld, Germany

<sup>4</sup> School of Mechanical Engineering, Shanghai Jiao Tong University (SJTU), Shanghai 200240, PR China

Published in Zeitschrift für Physikalische Chemie

<https://doi.org/10.1515/zpch-2020-1613>

## Abstract

Diethyl ether (DEE) has been proposed as a biofuel additive for compression-ignition engines, as an ignition improver for homogeneous charge compression ignition (HCCI) engines, and as a suitable component for dual-fuel mixtures in reactivity-controlled compression ignition (RCCI) engines. The combustion in these engines is significantly controlled by low-temperature (LT) chemistry. Fundamental studies of DEE LT oxidation chemistry and of its influence in fuel-mixture oxidation are thus highly important, especially at elevated pressures.

Elevated pressure speciation data were measured for the LT oxidation of DEE, of its similarly-structured linear five-heavy-atom hydrocarbon fuel (*n*-pentane), and of a mixture of the two fuels in a jet-stirred reactor (JSR) in the temperature range of 400-1100 K and at various pressures up to 10 bar. The pressure influence on the LT oxidation chemistry of DEE was investigated by a comparison of the measured profiles of oxidation products. The results for DEE and *n*-pentane were then inspected with regard to fuel structure influences on the LT oxidation behavior. The new speciation data were used to test recent kinetic models for these fuels [Tran *et al.*, Proc. Combust. Inst. 37 (2019) 511 and Bugler *et al.*, Proc. Combust. Inst. 36 (2017) 441]. The models predict the major features of the LT chemistry of these fuels well and could thus subsequently assist in the data interpretation. Finally, the LT oxidation behavior of an equimolar mixture of the two fuels was explored. The interaction between the two fuels and the effects of the pressure on the fuel mixture oxidation were examined. In addition to reactions within the combined model for the two fuels, about 80 cross-reactions between primary reactive species generated from these two fuel molecules were added to explore their potential influences.

**Keywords:** Low-temperature oxidation, diethyl ether, *n*-pentane, dual-fuel mixture, elevated pressure JSR.

## 1. Introduction

Diethyl ether (DEE) is of increasing interest as an additive for compression-ignition engines [1,2]. It has also been proposed as an ignition improver for HCCI engines [3], and as a component for dual-fuel mixtures in RCCI engines [4]. The combustion in these engines is significantly controlled by the low-temperature (LT) chemistry of the respective fuels. The numerical simulation of fuel-mixture combustion requires suitable models that must rely on well-established sub-mechanisms of each fuel component. Detailed, accurately determined kinetic data, especially in the LT regime, are necessary to develop these mechanisms. Moreover, reliable experimental data, especially species profiles, of neat fuels as well as fuel mixtures are a prerequisite to further develop and test such kinetic models. This need is especially acute for the elevated pressures relevant for the operation of practical engines. In this study, we provide new, extended sets of species mole fraction data for DEE and for its mixture with *n*-pentane ( $nC_5H_{12}$ ), a prototypical molecule for hydrocarbon fuels, in the temperature range of 400-1100 K and at pressures up to 10 bar. To ensure comparable conditions, respective datasets were obtained also for neat *n*-pentane.

Although the recent literature shows significant interest in the LT oxidation of DEE, focusing on ignition properties [5,6], species formation [7–9], and model development [7,8,10–13], only one study reporting species profiles [8] was performed at elevated pressure. While these authors [8] have determined about 12 species in a jet-stirred reactor (JSR) at 10 bar (and 1 bar) and discussed the fuel reactivity at elevated pressures, detailed analyses of the influence of pressure above 1 bar on the formation of LT oxidation products remain very limited.

To explore the influence of DEE's ether function, additional experiments with *n*-pentane that features similar linear five-heavy-atom structure were performed in the present study. While oxidation mechanisms of  $C_0$ - $C_4$  fuels were extensively investigated, that of heavier fuels need to be further inspected [14]. Therefore, these additional experiments with *n*-pentane contribute also to validate recent *n*-pentane mechanisms. Some studies about LT oxidation of *n*-pentane were reported [15–22]. However, Bugler *et al.* [15] have provided the only investigation reporting detailed speciation obtained at an elevated pressure above 1 bar. These data consist of mole fraction profiles of more than 30 species measured in a JSR at 10 bar (and 1 bar) and at temperatures of 500-1100 K using gas chromatography (GC) and Fourier transform infrared spectroscopy (FTIR). Comparative studies of the oxidation of DEE and *n*-pentane were previously reported for atmospheric pressure and focused mainly on the fuel reactivity or flammability limits [9,23] rather than on details of the species formation chemistry during the oxidation. Moreover, to the best of our knowledge, the LT oxidation of the mixture of DEE and *n*-pentane has not yet been investigated.

This study therefore has a three-fold objective: it aims at **(i)** enriching speciation data of both, DEE and *n*-pentane up to 10 bar and analyzing their elevated pressure LT oxidation chemistry as well as the *pressure* effects on the respective species formation; **(ii)** investigating influences of the *chemical structure* of DEE and *n*-pentane on the species formation behavior; and **(iii)** analyzing the oxidation of a *mixture* of these two fuels in a pressure range up to 10 bar.

## 2. Experiments

Experiments were performed in a JSR. Experimental conditions are summarized in Table 1. In total, four series of measurements were newly conducted at the same equivalence ratio  $\varphi=1$ , inlet fuel mole fraction of 0.005, and a residence time of 2 s. The first series was dedicated to the oxidation of DEE at 5 bar and temperatures of 400-1100 K. The second and third series

were performed for the oxidation of *n*-pentane in a temperature range of 500-1100 K at 5 bar and 10 bar, respectively. The fourth series investigated the oxidation of fuel mixtures at 650 K (the temperature of the highest fuel reactivity in the LT range) with pressures varied from 2.5 up to 10 bar.

**Table 1.** Experimental conditions.

Fuel	$\varphi$	P (bar)	$\tau$ (s)	T (K)	Inlet mole fraction				C/O
					He	O <sub>2</sub>	DEE	<i>n</i> -Pentane	
DEE	1	5	2	400-1100	0.965	0.03	0.005	0	0.308
<i>n</i> -Pentane	1	5, 10	2	500-1100	0.955	0.04	0	0.005	0.313
DEE/ <i>n</i> -pentane	1	2.5-10	2	650	0.960	0.035	0.0025	0.0025	0.310

Flow rates of liquid fuels (Sigma-Aldrich, purity >99%) were controlled using a Coriolis flow controller followed by an evaporator. The flow rates of helium (Messer, 99.99%) and oxygen (Messer, 99.999%) were controlled by Bronkhorst mass flow controllers. The liquid fuel mixture (DEE/*n*-pentane: 50%/50% on a molar basis) was prepared by weighting the requested quantities and mixing them in the same vessel. We considered that the fraction of fuels and the homogeneity of this mixture in both gas and liquid phases are crucial parameters, therefore they were cross-checked using two independent techniques, *i.e.* GC instruments in Nancy (for the fuel mixture in liquid and gas phases) and a nuclear magnetic resonance (NMR) spectroscopy device in Bielefeld with higher accuracy (for the same liquid mixture sample that was transported from Nancy). Details of the resulting NMR spectrum and its corresponding description are available in Supplementary Material 1 (SM1), Fig. S1. Uncertainties in mixture preparation were thus determined to be <6% based on GC experiments and ~0.3% based on NMR experiments, demonstrating that the prepared fuel mixture was very fine.

Oxidation products were analyzed mainly using the GC technique. Since details of the JSR-GC system were previously described in [24], only the main features of the experimental apparatus are summarized below. The JSR (60 cm<sup>3</sup> volume) was made of fused silica and heated by Thermocoax resistances rolled up around it. The reaction temperature was measured by a thermocouple (type K) located in the intra-annular part of the preheating with its extremity in a glass finger entering slightly inside the spherical part. The JSR outlet was directly connected to three GC instruments, allowing online analyses of oxidation products. The GC systems were equipped with three columns (Carbosphere, PlotQ, and HP-5 columns) and three detectors (a thermal conductivity detector, a flame ionization detector coupled to a methanizer for quantification, and a mass spectrometric detector with electron ionization at 70 eV for identification). Calibration factors were determined using cold-gas mixtures when available. For other species, calibration factors were determined relying on hydrogenation by the methanizer, to be identical to those of the alkanes with the same number of carbon atoms. This procedure has been successfully used before [7,25] with estimated uncertainties of <15%. Carbon atom balances were checked (see SM3) and found to be good (1.0±10%), even in the low-temperature oxidation region, meaning that most reaction products were detected during the study. Oxygen atom balances are also good under unreactive conditions, but deteriorate under reactive conditions mainly due to the fact that water was not quantified.

Species quantification reported in this paper relies exclusively on the GC experiments. To confirm species identification, however, we used a second JSR (designed for atmospheric pressure) coupled to a tunable synchrotron vacuum ultraviolet (VUV) photoionization molecular-beam mass spectrometry (PI-MBMS) instrument located at the National

Synchrotron Radiation Laboratory (NSRL) in Hefei, China. These identification experiments were performed at 1 bar for selected species in the oxidation of both neat fuels and the mixture of DEE and *n*-pentane. The apparatus at the NSRL has been previously described in [26]. Briefly, gas samples were extracted from the JSR by a quartz sampling nozzle. The resulting molecular beam was then intersected and ionized by the tunable synchrotron VUV light. The ions were transferred by an ion guide to a home-made reflectron time-of-flight mass spectrometer (TOF-MS) with a mass-resolving power ( $m/\Delta m$ ) of  $\sim 2500$ . Photoionization efficiency (PIE) spectra were measured in a photon energy range of 8–11.5 eV, with uncertainties in the determination of ionization energies of  $\pm 0.05$  eV and  $\pm 0.10$  eV for strong and poor signal-to-noise ratio, respectively. While the PIE results for DEE at 1 bar were already used in the previous study [7], those for *n*-pentane and the fuel mixture were newly obtained in the present study. PIE curves were measured for several reactor temperatures. Comparisons of PIE curves between DEE, *n*-pentane, and the fuel mixture for some species are exemplarily presented in SM1 (Fig. S2).

### 3. Modeling

Several (at least six) kinetic models for the LT oxidation of DEE are available in the literature [7,8,10–13]. In the present study, these models were preliminarily tested against the present LT data and that of [7,8]. The model developed previously in [7] predicted the fuel reactivity quite well, especially much better than other models, under the present study's conditions (see SM1, Fig. S3). This model [7] was thus used in the current analyses. Note that this DEE model was already implemented (during the previous work by Tran *et al.* [7]) into the *n*-pentane model of the NUI-Galway group [15]. Therefore, the use of this model allows us to simulate DEE, *n*-pentane, and their mixtures with the same model.

Although the reaction subsets of DEE and *n*-pentane were described previously in [7] and [15], respectively, it is deemed useful here to provide some information on important aspects regarding these sub-mechanisms. The reaction subset of DEE includes both high-temperature (HT) and LT chemistries, which were already tested against several experimental data including flame speeds [27–30], ignition delay times (IDTs) [6,31], pyrolysis species [31,32], flame species profiles [27,33], and LT JSR and plug-flow reactor (PFR) species profiles [7]. In the present study, the DEE model of [7] has also been tested with the 10 bar JSR data of Serinyel *et al.* [8] and shows an overall appropriate prediction capability (see Fig. S4). The HT reaction subset includes 7 major classes of elementary reactions, while the LT reaction subset includes 31 main elementary reaction classes (the details for those reaction classes are available in [7]). A particular point in this DEE mechanism is the consideration of the formation paths of acetic acid ( $\text{CH}_3\text{COOH}$ ) and acetic anhydride (AA,  $(\text{CH}_3\text{CO})_2\text{O}$ ) from DEE-specific ketohydroperoxides. Regarding the *n*-pentane mechanism [15], it also includes major classes of elementary reactions for both HT and LT chemistries with several similarities to those considered for DEE. Bugler *et al.* [15] improved the *n*-pentane mechanism based on their previous model [34] to account for the formation of  $\text{C}_5$  oxygenated species at LT, and the model was previously examined against experimental data of ignition delay times (IDTs) [34–37], flame speeds [38], and JSR species profiles [15]. In the present study, the *n*-pentane model was further tested with new LT species profiles obtained in the JSR at elevated pressure (5 bar and 10 bar).

In the initial model version [7], DEE and *n*-pentane chemistries interact together only through the reactions of small species (H, OH,  $\text{CH}_3$ , CO, *etc.*). To investigate the role of cross-reactions between the initially generated, primary radicals of both fuels, we have thus added

about 80 such cross-reactions of primary fuel-specific radicals. These cross-reactions have been considered for a number of reaction classes: **(i)** H-abstraction reactions from fuels (by fuel radicals R, other fuel-specific radicals, and ROO radicals) with rate coefficients mainly estimated using rate rules [39]; **(ii)** reaction class  $R+ROO=RO+RO$ , **(iii)** reaction class  $R+C_2H_5O_2=RO+C_2H_5O$  ( $R=C_5H_{11-1, -2, -3}$ ); **(iv)** reaction class  $ROO+ROO=RO+RO+O_2$ ; and **(v)**  $ROO+ROO=carbonyl+alcohol+O_2$ . The rate coefficients of these latter reactions were estimated by analogy to similar reactions in the model, with details available in SM2. To explain the approach exemplarily, consider reaction class **(ii)**: here, four different combinations with R derived either from DEE or from *n*-pentane are possible, of which two (for each neat fuel) are already included in the model, whereas the other two (between one radical derived from the first fuel and the other from the second one) are cross-reactions that were added. Also, in case **(iii)**, note that  $C_2H_5$  is a radical that can be formed in the oxidation of each neat fuel; however, it is a primary radical in DEE decomposition and cross-reactions of its peroxy radical (ethyl peroxy radical,  $C_2H_5O_2$ ) with the three isomeric primary fuel radicals from *n*-pentane ( $C_5H_{11}$ ) must be considered.

We will refer to the kinetic model including these cross-reactions as the “**present model**”. Its related files (reaction kinetic, thermodynamic, and transport data) are available in CHEMKIN format in SM2. Note that the newly-added cross-reactions do not influence simulations with individual fuel (*i.e.* either DEE or *n*-pentane). Therefore, simulation profiles in their respective figures that are presented in this paper are identical between the present model and the model of [7]. Potential effects of these newly-added cross-reactions on simulations for the fuel mixture will be discussed later in the paper.

## 4. Results and discussion

Elevated pressure LT oxidation of DEE will be discussed in Section 4.1. A comparison of the oxidation behavior between *n*-pentane and DEE will be presented in Section 4.2. The oxidation of the DEE–*n*-pentane mixture will be addressed in Section 4.3. The experimental data are available in tabulated format in SM3.

### 4.1. Elevated pressure LT oxidation of DEE

The main objective of this section is to reveal the elevated pressure LT oxidation of DEE. New experimental speciation data for the oxidation of DEE at 5 bar were thus measured, which consist of the mole fraction profiles of 19 species. These include reactants (DEE,  $O_2$ ), CO,  $CO_2$ , 2  $C_1$  intermediates, 7  $C_2$  species, 2  $C_3$  species, and 4  $C_4$  intermediates species. Many of the detected species are LT fuel-specific intermediates, *i.e.* species produced by the LT primary mechanism of DEE. This new experimental speciation data of DEE was then used to test the present model and analyzed the elevated pressure LT oxidation of DEE as will be discussed in the coming paragraphs for major and intermediate species. To permit comparison, the previous 1 bar data ( $\varphi=1.0$ , inlet DEE mole fraction of 0.01, and residence time of 2 s) [7] are added in figures of this section. Every profile is normalized by the inlet mole fraction of DEE in the specific experiment to ensure comparable scales between the measurements. Since the inlet DEE mole fraction which is different between the present experiments (DEE at 5 bar: 0.005) and the previous ones (DEE at 1 bar: 0.01) could influence the reactivity and product formation, simulations were also performed for 1 bar with a DEE mole fraction of 0.005. Although the absolute mole fraction of some species is changed, the different initial fuel contents have no significant impact on the relative trends between 1 bar and 5 bar (see

examples in SM1, Fig. S5). The 1 bar data of [7] may thus be considered for further inspection of the elevated pressure effect of the DEE LT chemistry in this section.

#### 4.1.1. Main species

Figure 1 presents the mole fraction profiles as a function of temperature of DEE (a), CO (b), and CO<sub>2</sub> (c). The new results from the present work confirm that DEE is very reactive and starts to react at a relatively low temperature of about 450 K. Pressure does not affect significantly this start of DEE consumption (Fig. 1a), but increasing pressure increases strongly the global reactivity. For example, at 750 K, ~80% of DEE is consumed at 5 bar while only ~30% of DEE is consumed at 1 bar (Fig. 1a). Accordingly, the mole fractions of CO and CO<sub>2</sub> increase in 5 bar oxidation (Fig. 1b,c). The enhancement of fuel reactivity with increasing pressure is expected because O<sub>2</sub> addition reactions are favored when increasing the pressure. Negative temperature coefficient (NTC) zones (525-600 K and 650-725 K) are weak, especially at 5 bar where only a change of slope is noted in the DEE profile in the range of the first NTC zone at 525-600 K. The occurrence of two NTC zones during the LT oxidation of DEE at 1 bar was extensively explained in [7], and the discussion is thus not repeated here. Overall, the present model predicts the fuel consumption well and captures the experimental trends appropriately. However, a slight under-prediction of the DEE reactivity at 5 bar starting at 550 K is noted, and the first NTC still appears in the simulation at this pressure. This simulated first NTC results mainly from a competition between the  $\beta$ -scission of the C-O bond of the Q10OH radical (*i.e.* Q10OH  $\rightarrow$  CH<sub>3</sub>CHO + CH<sub>3</sub>CHO + OH) and the second O<sub>2</sub> addition (*i.e.* Q10OH + O<sub>2</sub>  $\rightleftharpoons$  OOQ10OH). The structures of Q10OH, OOQ10OH, and these reactions are referred to below in Section 4.1.2. (Fig. 2a). As a short test to inspect potential reasons for the noted differences between experiment and simulation, we reduced the branching ratio between these two reactions by a factor of two. The result of this test shows the first NTC to be quite suppressed at 5 bar, similar to the experimental observations, while the model still reflects the two NTC zones well for 1 bar profiles. However, such fitting of individual reaction coefficients for improving agreement between the model and the experiment is an approach that cannot provide further fundamental insight. Therefore, we kept the original rate coefficients of [7] for the present model. A comprehensive inspection of the branching ratio of these reactions at different pressures using high-level theoretical calculations will be a useful and interesting topic of future study beyond the scope of this investigation.

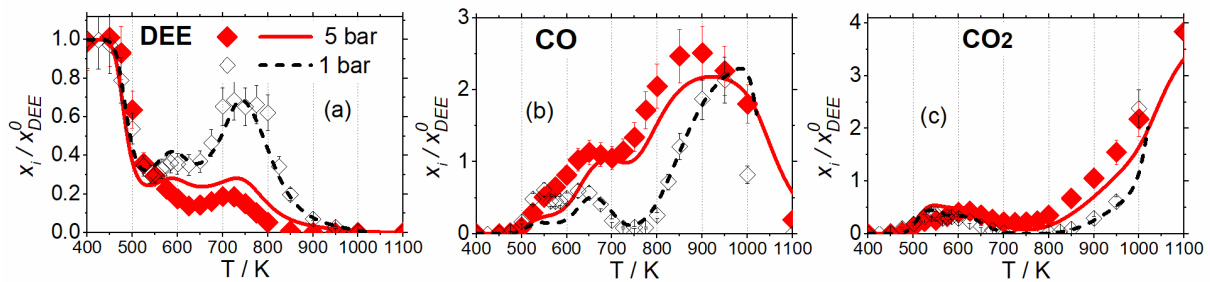


**Fig. 1.** Profiles of mole fraction ( $x_i$ ) of DEE (a), CO (b), and CO<sub>2</sub> (c) (normalized by the inlet fuel mole fraction,  $x_{DEE}^0$ ) obtained at 5 bar as a function of temperature. The results obtained at 1 bar [7] are shown for comparison. Both datasets were taken at  $\phi=1.0$  and residence time of 2 s. *Symbols:* experiment, *lines:* present model.

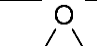
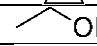
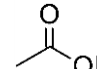
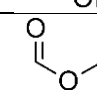
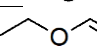
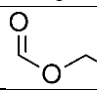
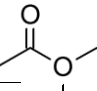
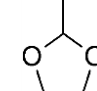
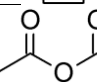
#### 4.1.2. Intermediate species

Table 2 provides an overview by reporting the name and structure of the measured intermediate species as well as their peak mole fractions together with the temperature at which their respective maximum mole fraction occurs. This table shows that the oxidations at elevated pressure and 1 bar have similar species categories based on temperature criteria. For example, at both pressures, all detected hydrocarbons ( $\text{CH}_4$ ,  $\text{C}_2\text{H}_4$ ,  $\text{C}_2\text{H}_6$ ,  $\text{C}_3\text{H}_6$ ) and ethylene oxide ( $\text{C}_2\text{H}_4\text{O-cy}$ ) reach their maximum mole fractions in a HT range (from 800 K, beyond the second NTC), indicating that they are significantly produced *via* either HT chemistry or secondary reactions.  $\text{CH}_4$  and  $\text{C}_2\text{H}_4$  are the most abundant species of this category. Formaldehyde ( $\text{CH}_2\text{O}$ ), acetaldehyde ( $\text{CH}_3\text{CHO}$ ), ethyl vinyl ether (EVE), ethyl formate (EF), and 2-methyl-1,3-dioxolane ( $\text{C}_4\text{H}_8\text{O}_2\text{-cy}$ ) reach their peak mole fractions in a temperature range of 550-750 K, in which NTC zones occur (see Fig. 1a).  $\text{CH}_2\text{O}$  and  $\text{CH}_3\text{CHO}$  were measured with quite high amounts in this category. Finally, acetic acid ( $\text{CH}_3\text{COOH}$ ), ethyl acetate (EA), and acetic anhydride (AA) reach their mole fractions in a relatively low temperature range (<550 K) in which the DEE reactivity increases strongly with increasing temperature. Among these latter species,  $\text{CH}_3\text{COOH}$  occurs with very high mole fraction, about 10-100 times higher than other species, confirming that this species is an important intermediate of LT DEE oxidation at both elevated and atmospheric pressures.

Regarding the influence of pressure on these intermediate species, it can be noted that when increasing the pressure from 1 bar to 5 bar, species formation is affected differently (Table 2 and Fig. S6); it is either inhibited (classified as the “first group”, such as  $\text{C}_2\text{H}_4$ ,  $\text{C}_2\text{H}_6$ ,  $\text{C}_2\text{H}_4\text{O-cy}$ , EVE) or enhanced (second group, such as  $\text{C}_2\text{H}_5\text{OH}$ , MF,  $\text{CH}_3\text{COOH}$ , EF, EA, AA) or insignificantly influenced (third group, such as  $\text{CH}_4$ ,  $\text{CH}_2\text{O}$ ,  $\text{C}_3\text{H}_6$ ,  $\text{CH}_3\text{CHO}$ ,  $\text{C}_4\text{H}_8\text{O}_2\text{-cy}$ ). Peak mole fractions of the species of the first group experiencing inhibition appear at quite high temperatures, while those of species in the second group that are enhanced appear at lower temperature. Their occurrence at LT and increase with increasing pressure suggests that they could be produced along with the pathways of  $\text{O}_2$  additions. Species in the first group, conversely, could be mainly formed along with routes that are in competition with  $\text{O}_2$  additions, such as  $\beta$ -scissions. The third group species could be influenced by both these routes or by reaction paths that are less sensitive to pressure. Of course, these arguments should be applicable only for fuel-decomposition species that are mostly controlled by primary reactions, the main focus of the present study; they may not be viable for secondary species because these species depend in a complex way on secondary reactions.

**Table 2:** Nomenclature, name, and structure of intermediate species in DEE oxidation together with their experimental peak mole fractions  $x_{max}$  (normalized by the inlet DEE mole fraction,  $x_{DEE}^0$ ). M: nominal mass. T: temperature at  $x_{max}$  (K). The results obtained at 1 bar [7] are shown for comparison.

M	Nomenclature	Name	Structure	5 bar		1 bar [7]		Group <sup>a</sup>
				$x_{max}/x_{DEE}^0$	T	$x_{max}/x_{DEE}^0$	T	
16	$\text{CH}_4$	Methane	$\text{CH}_4$	2.2E-01	800	2.0E-01	900	third
28	$\text{C}_2\text{H}_4$	Ethylene	$\text{=}$	2.0E-01	800	4.8E-01	850	first
30	$\text{C}_2\text{H}_6$	Ethane	$\text{—}$	1.1E-02	800	2.3E-02	850	first
	$\text{CH}_2\text{O}$	Formaldehyde	$\text{=O}$	2.2E-01	575/725 <sup>b</sup>	1.9E-01	600	third
42	$\text{C}_3\text{H}_6$	Propene	$\text{>}$	4.0E-03	800	5.2E-03	850	third
44	$\text{CH}_3\text{CHO}$	Acetaldehyde	$\text{>=O}$	6.0E-01 <sup>c</sup>	700	6.1E-01 <sup>c</sup>	650	third

	C <sub>2</sub> H <sub>4</sub> O-cy	Ethylene oxide		6.1E-03	800	9.7E-03	850	first
46	C <sub>2</sub> H <sub>5</sub> OH	Ethanol		3.6E-03	500 <sup>d</sup>	2.0E-03	600 <sup>d</sup>	second
60	CH <sub>3</sub> COOH	Acetic acid		5.8E-01	525	2.8E-01	525	second
	CH <sub>3</sub> OCHO, MF	Methyl formate		2.0E-03	575	1.1E-03	525	second
72	C <sub>4</sub> H <sub>8</sub> O, EVE	Ethyl vinyl ether		5.8E-04	700	2.1E-03	700	second
74	C <sub>3</sub> H <sub>6</sub> O <sub>2</sub> , EF	Ethyl formate		1.8E-02	550	1.2E-02	500	second
88	C <sub>4</sub> H <sub>8</sub> O <sub>2</sub> , EA	Ethyl acetate		4.1E-03	525	2.8E-03	525	second
	C <sub>4</sub> H <sub>8</sub> O <sub>2</sub> -cy	2-Methyl-1,3-dioxolane		1.5E-02	675	1.8E-02	625	third
102	C <sub>4</sub> H <sub>6</sub> O <sub>3</sub> , AA	Acetic anhydride		4.8E-02	525	1.6E-02	500	second

Note: <sup>a</sup> First, second, and third groups indicate species that were inhibited, enhanced, and insignificantly influenced, respectively, when increasing the pressure from 1 bar to 5 bar. This relative comparison took into account the experimental uncertainty of both mole fraction values, assuming conservatively an uncertainty range of  $\pm 30\%$  (for a 15% error associated with an individual value) (see Fig. S6 for a graphic visualization of this comparison). <sup>b</sup> Two equivalent peaks. <sup>c</sup> Including a fraction of methanol because the used GC system could not separate it from acetaldehyde. <sup>d</sup> Peak tailing, ambiguous peak location.

The further discussion in this section will thus focus on selected examples of detected intermediate species formed in the fuel decomposition. Figure 2 presents DEE reaction pathways (a) based on the present model and the mole fraction profiles of related fuel-decomposition species (b-g). Mole fraction profiles of other species are available in SM1 (Fig. S7). Figure 2a shows that DEE is largely consumed by H-abstraction reactions by small radicals X\* (OH, CH<sub>3</sub>O, H, etc.) at C<sub>α</sub> (neighboring the ether group of DEE), yielding the initial fuel radical R1, while H-abstractions at C<sub>β</sub> position (next to C<sub>α</sub>) account only for 6-8% of DEE consumption, yielding the initial fuel radical R2. H-abstractions by OH and CH<sub>3</sub>O are significant under the analysis conditions and account for 60-90% and 15-25%, respectively, of DEE consumption. R1 and R2 in turn produce C<sub>2</sub>H<sub>4</sub>, CH<sub>3</sub>CHO, CH<sub>3</sub>COOH, C<sub>4</sub>H<sub>8</sub>O<sub>2</sub>-cy, EA, and AA *via* different stages. The experimental mole fraction profiles of the three latter species were not reported previously in any elevated pressure DEE study in the literature. Overall, despite some deviations, the present model reproduces quite well major trends for mole fraction profiles of these species at both studied pressures (Fig. 2b-g). For example, good agreement is seen between the model and the experiment for the absolute peak mole fraction of EA (Fig. 2f), although the present model under-predicts the formation of this species in the higher temperature range at 5 bar. This observation indicates that a revision of its formation reactions (*e.g.*, R100+R100, Fig. 2a) could be necessary to improve the prediction of this species in the higher temperature range. However, more accurate kinetic data of such reactions are not available.



While the  $C_2H_4$  peak position (Fig. 2b) is predicted quite well by the model, its absolute mole fraction at 5 bar is significantly over-predicted. To understand this discrepancy, rate of production analyses with the present model in a temperature range of 650-900 K for both pressures were performed. The results indicate that while only a small part of  $C_2H_4$  (<10%) is produced by the C-O  $\beta$ -scission of the R2 radical (Fig. 2a), this species is mostly produced from  $C_2H_5$  chemistry (through the following reactions:  $C_2H_5+O_2\rightarrow C_2H_5O_2\rightarrow C_2H_4+HO_2$  and  $C_2H_5+O_2\rightarrow C_2H_4+HO_2$ ). The  $C_2H_5$  radical is mainly produced from the R1 radical *via* the reaction  $R1\rightarrow C_2H_5+CH_3CHO$  (Fig. 2a). As a test, we reduced the rate coefficient of the latter reaction by a factor of 2 (within the calculation uncertainty), and resulting simulations indicate that  $C_2H_4$  reduces only by 6%, indicating that the  $C_2H_4$  formation is not strongly sensitive to this reaction, and reactions in  $C_2H_5$  chemistry of the core model could be a subject for examination. Similarly, the  $CH_2O$  prediction in the LT range (Fig. S7) could be improved by considering the reaction  $CH_3O_2+CH_3CO_3\rightarrow CH_3COOH+CH_2O+O_2$  that is missing from the core model. Improvement of the core model is beyond the objective of the present study, however. Despite these discrepancies, the model predicts the relative trends between 5 bar and 1 bar quite well, allowing further analyses of the influence of elevated pressure.

Figure 2a shows that at higher temperature, a large fraction of R1 is consumed by C–O  $\beta$ -scission forming  $CH_3CHO$  and  $C_2H_5$  which is the source of  $C_2H_4$ . At lower temperature, *e.g.* 500 K and 560 K, R1 reacts largely by the first  $O_2$  addition leading to the formation of the R1OO radical. The consumption ratio between these two paths (first  $O_2$  addition/ $\beta$ -scission of R1) increases with increasing pressure (for example, at 560 K this ratio is 24 for 5 bar vs. 12 at 1 bar), explaining the reduction of the mole fractions of  $C_2H_4$  with pressure. R1OO isomerizes then to the Q1OOH radical that decomposes by  $\beta$ -scission to form two  $CH_3CHO$  molecules or reacts by a second  $O_2$  addition to form the OOQ1OOH radical. Subsequent reactions of OOQ1OOH lead to the production of AA,  $CH_3CHO$ , and  $CH_3COOH$ . Again, the consumption ratio between the second  $O_2$ -addition and the  $\beta$ -scission of Q1OOH increases, by a factor of 2-3, when increasing the pressure from 1 bar to 5 bar, explaining why AA and  $CH_3COOH$  mole fractions increase accordingly. As it can be seen,  $CH_3CHO$  can be produced *via* both  $\beta$ -scissions and  $O_2$ -additions, explaining why it was detected at LT and HT, and why its mole fraction profiles are not significantly affected by pressure.

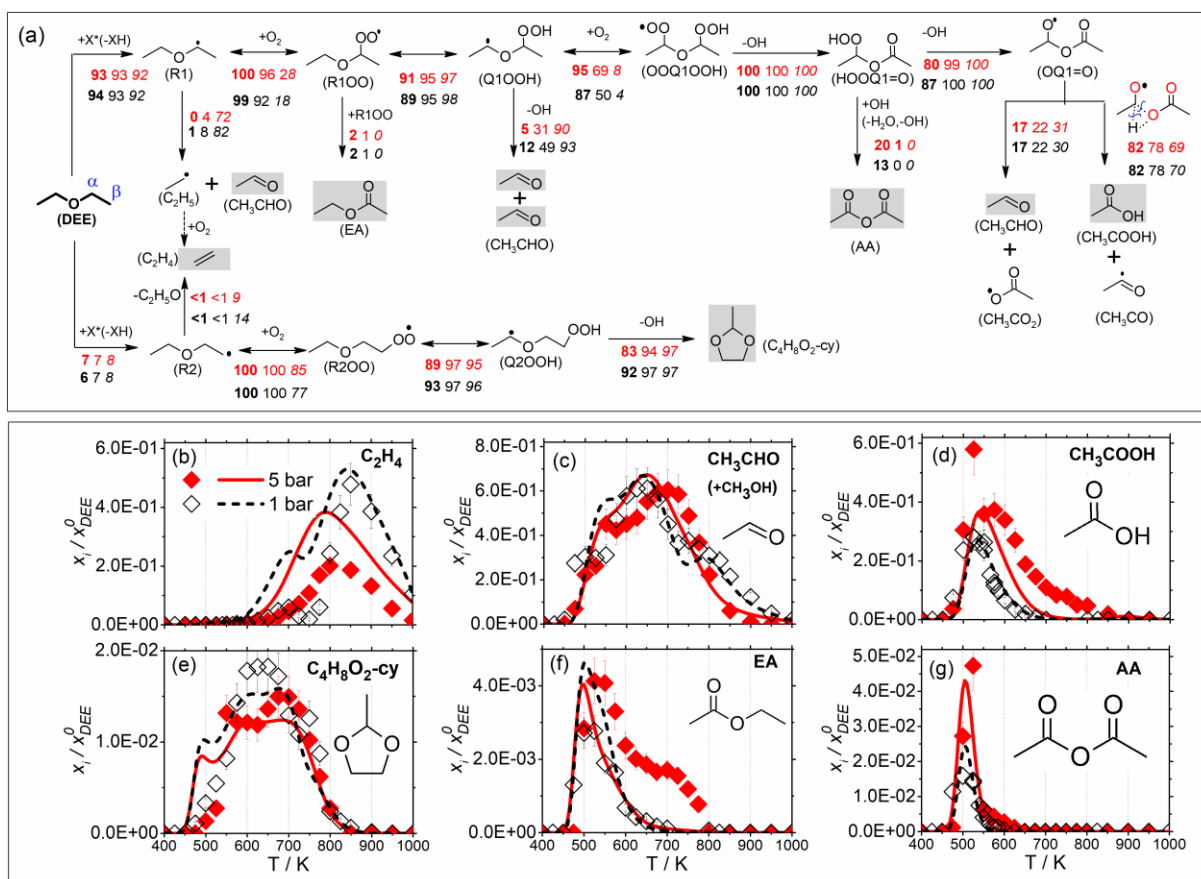


**Fig. 2.** (a) Diagram of reaction pathways for DEE. The species highlighted by shadowed squares have been quantified experimentally (see b-g). The numbers are percent contribution to the consumption of the species on the source side at different temperatures (coded with different fonts: **bold**: 500 K, normal: 560 K, *italic*: 715 K) and calculated based on the present model for 5 bar (*upper row*) and 1 bar (*lower row*) under the studied JSR conditions. (b-g): Profiles of mole fraction ( $x_i$ ) of selected species obtained at 5 bar. Data at 1 bar [7] are added for comparison. Values for both datasets were normalized by the inlet fuel mole fraction,  $x_{DEE}^0$  and taken at  $\phi=1.0$  and a residence time of 2 s. Symbols: experiment, lines: present model.

#### 4.2. Comparison of the LT oxidation of DEE and *n*-pentane

The aim of this section is to reveal the influence of the chemical structure of the two fuels on their elevated pressure LT oxidation behavior, by comparing DEE and *n*-pentane data obtained in the present study under identical conditions ( $\phi=1.0$ , 5 bar, inlet fuel mole fraction of 0.005, compare Table 1).

Prior to using them in the comparative study with DEE, the experiments and the model of *n*-pentane were compared with an aim to test the chosen *n*-pentane model [15] against the elevated pressure data obtained under the present JSR conditions. About 36 species were experimentally identified and quantified for *n*-pentane oxidation at 5 bar and 10 bar. These species include reactants, CO, CO<sub>2</sub>, 2 C<sub>1</sub> intermediate species, 6 C<sub>2</sub> species, 5 C<sub>3</sub> species, 7 C<sub>4</sub> species, and 12 C<sub>5</sub> species including 6 C<sub>5</sub>H<sub>10</sub>O isomers. A very good agreement between the experiments and the model was observed, lending confidence to our choice of this model for

the analysis of *n*-pentane oxidation. Some important examples of species profiles are provided in SM1 (Figs. S8 and S9). The oxidation of DEE and *n*-pentane is now compared in the following, using the data of 5 bar.

Figure 3 presents the mole fraction profiles of fuels, CO, and CO<sub>2</sub>. Figure 3a confirms DEE to be much more reactive than *n*-pentane. DEE starts to react at a temperature that is 100 K lower than that for *n*-pentane, and it has a higher conversion rate (for example, at 650 K, DEE conversion is ~90%, while *n*-pentane conversion is ~60%). The LT chemistry of DEE occurs in a larger temperature range (450-725 K vs. 550-725 K for *n*-pentane). Although DEE starts to react at much lower temperature than *n*-pentane, both fuels have an NTC zone located over a similar range of temperatures (650-725 K). The NTC of DEE is much less pronounced, however. Furthermore, although it is quite weak at 5 bar, the first NTC zone for DEE still exists (525-600 K, Fig. 3a), while such behavior cannot be seen for *n*-pentane. The present kinetic model reflects all trends described above very well. Figures 3b,c show that the mole fraction profiles of CO and CO<sub>2</sub> evolve somewhat differently in LT ranges between the two fuels, but they reach close maximal mole fractions for the two fuels, which is consistent with the initial C/O ratio (~0.31, compare Table 1).

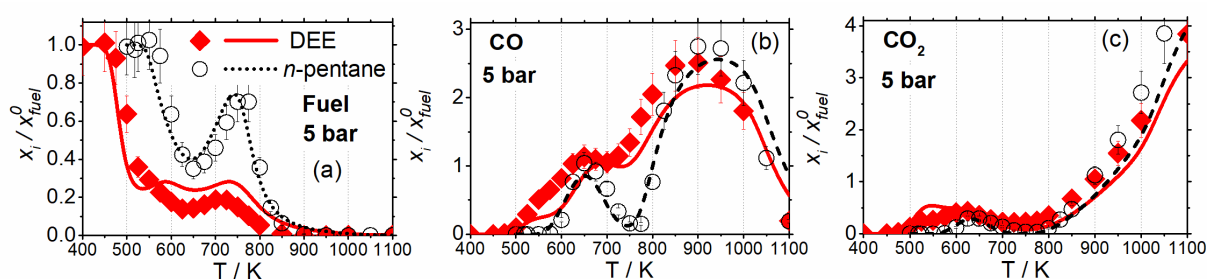


**Fig. 3.** Comparison between DEE and *n*-pentane (5 bar,  $\phi=1.0$ , and residence time of 2 s): profiles of fuels (a), CO (b), and CO<sub>2</sub> (c). *Symbols:* experiment, *lines:* present model. Normalized by the specific inlet fuel mole fraction,  $x_{fuel}^0$ . Because of the same inlet fuel mole fraction (*i.e.* 0.005), this normalization is performed just to be consistent with figures presented in Section 4.1.

Figures 4 present the chemical structure of DEE and *n*-pentane (a), an analogous reaction diagrams explaining the occurrence of the NTC zone of 650-725 K for the two fuels (b), and sensitivity analyses for the consumption of these fuels in this NTC zone using the present model (c,d). Figure 4a shows that the presence of an O-atom in DEE's structure lowers the bond dissociation energy (BDE) of secondary C-H bonds, which favors H-abstractions from DEE and facilitates the reactions R10O→Q1OOH and OOQ1OOH→OH+HOOQ1=O (*cf.* reaction paths shown in Fig. 2a), resulting in a higher reactivity for DEE. Regarding their chemical structure, analogous reaction diagrams can be drawn for DEE and *n*-pentane (Fig. 4b) to explain the occurrence of the NTC zone (650-725 K). The  $\beta$ -scission of fuel radicals R1 (reaction *r1* in Fig. 4b) and HO<sub>2</sub> elimination from R10O (reaction *r3*) reduce the fuel reactivity because they compete with first O<sub>2</sub> addition (reaction *r2*) and isomerization of R10O (reaction *r4*), respectively. Sensitivity analyses with the present model enable several conclusions in line with the discussions above. They confirm, firstly, that in DEE oxidation (Fig. 4c), the  $\beta$ -scission of fuel radicals ( $C_2H_5OC_2H_4-A \rightleftharpoons C_2H_5+CH_3CHO$ ) and the subsequent reactions of the resulting C<sub>2</sub>H<sub>5</sub> radical ( $C_2H_5+O_2 \rightleftharpoons HO_2+C_2H_4$ ,  $C_2H_5O_2 \rightleftharpoons HO_2+C_2H_4$ ) inhibit DEE consumption, which is similar to the behavior observed at 1 bar [7]. Secondly in the oxidation of *n*-pentane (Fig. 4d), HO<sub>2</sub> eliminations from the R10O radicals ( $C_5H_{11}O_2-2 \rightleftharpoons HO_2+C_5H_{10}-1$  and  $C_5H_{11}O_2-$

$2 \rightleftharpoons \text{HO}_2 + \text{C}_5\text{H}_{10-2}$ ) reduce *n*-pentane's reactivity, which is consistent with previous observations [34]. Thirdly, these analyses reveal that even if they exhibit analogous major reaction pathways, the mechanisms for the occurrence of the NTC zone between DEE and *n*-pentane present some significant differences because of the influence of the ether group in DEE.

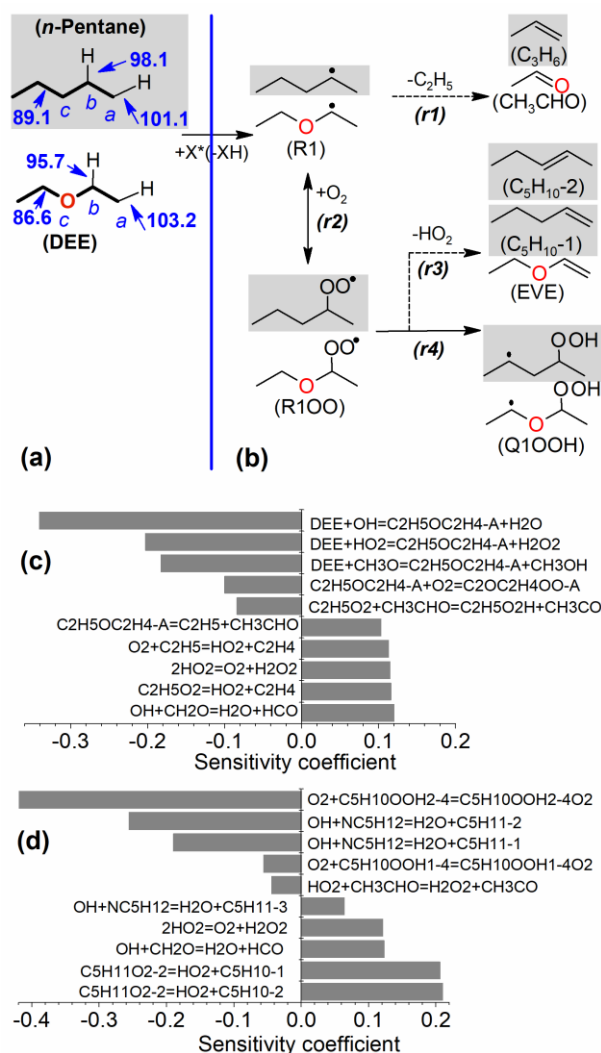


**Fig. 4.** (a) Fuel structures; numbers in **bold** font on fuel structure are bond energies in kcal mol<sup>-1</sup> [15,27]. (b) Analogous reaction diagrams for the occurrence of the NTC zone (650-725 K). Only one fuel radical (R1) of each fuel is presented exemplarily. Species of *n*-pentane oxidation are highlighted by shadowed squares; non-highlighted ones are for DEE. (c,d) Sensitivity analyses at 715 K (5 bar,  $\phi=1.0$ , and residence time of 2 s) for the consumption of DEE and *n*-pentane, respectively. Negative coefficients indicate a reaction which promotes the computed fuel consumption and vice versa. Chemical nomenclatures in (c,d) correspond to assignments in the CHEMKIN format kinetic mechanism. For reading facility, nomenclature for some specific species is explained here: C2H5OC2H4-A in (c) and C5H11-2 in (d) are R1 in (b), NC5H12 in (d) is *n*-pentane in (a), C2OC2H4OO-A in (c) and C5H11O2-2 in (d) are R1OO in (b), C5H10OOH2-4 in (d) is Q1OOH in (b).

Regarding the species distribution, about 36 species were detected for *n*-pentane, while only 19 species were detected for DEE. In the oxidation of DEE, C<sub>2</sub> species are the most numerous ones (7 species) while C<sub>5</sub> species (12 species) are predominant in *n*-pentane

oxidation, which confirms that the C-O bonds of DEE are easier broken than the corresponding C-C bonds of *n*-pentane (see BDEs in Fig. 4a). Small species in the C<sub>1</sub> to C<sub>3</sub> range, such as CO, CO<sub>2</sub>, CH<sub>4</sub>, CH<sub>2</sub>O, C<sub>2</sub>H<sub>4</sub>, C<sub>2</sub>H<sub>6</sub>, C<sub>3</sub>H<sub>6</sub>, C<sub>2</sub>H<sub>4</sub>O-cy, CH<sub>3</sub>CHO, C<sub>2</sub>H<sub>5</sub>OH, and CH<sub>3</sub>COOH, were commonly detected for both fuels. While CO and CO<sub>2</sub> were already shown in Fig. 3, profiles of other species are presented in Fig. S10. Somewhat similar maximal mole fraction values between DEE and *n*-pentane oxidation are noted for CH<sub>4</sub>, CH<sub>2</sub>O, and C<sub>2</sub>H<sub>6</sub>, whereas *n*-pentane produces C<sub>2</sub>H<sub>4</sub> and C<sub>3</sub>H<sub>6</sub> in higher mole fractions, and DEE produces CH<sub>3</sub>CHO and CH<sub>3</sub>COOH in distinctly higher mole fractions.

Regarding intermediates including at least 4 carbon atoms, those detected for *n*-pentane are different in structure from those measured for DEE, therefore direct comparisons are not possible. A comparison based on the nature of the fuel decomposition is therefore proposed here to reveal further potential differences or similarities between the oxidation of these two fuels. Exemplarily, Fig. 5 presents possible analogous reaction pathways from DEE and *n*-pentane leading to the formation of cyclic ethers (a) and of diones, acetone, and acetic acid (b). Mole fraction profiles of these species are added into the corresponding figures. Figure 5a shows that 2-methyltetrahydrofuran (MTHF) and 2-methyl-1,3-dioxolane (C<sub>4</sub>H<sub>8</sub>O<sub>2</sub>-cy) can be produced by a similar mechanism *via* H-abstractions of primary H-atoms of *n*-pentane and DEE, respectively. C<sub>4</sub>H<sub>8</sub>O<sub>2</sub>-cy is formed in lower mole fraction than MTHF, however. Figure 5b shows that AA and CH<sub>3</sub>COOH, species of DEE oxidation, were detected with much higher amounts than 2,4-pentanedione (NC5dione24) and acetone (CH<sub>3</sub>COCH<sub>3</sub>), the related species produced during *n*-pentane oxidation, respectively, although these products have analogous formation mechanisms (*via* the second O<sub>2</sub> additions starting with Q1OOH), which again highlights a significant influence of the O-atom in the chemical structure of DEE. Regarding CH<sub>3</sub>COOH in DEE oxidation, it is found to be exclusively produced from OQ1=O by the formation path presented in Fig. 5b. As recently discussed in [7,40], this reaction class is significant in the LT oxidation of ether fuels. This pathway involves the interaction of a hydrogen atom with the oxygen of the ether function and the breaking of the adjacent C-O bond (see Fig. 5b) and is promoted by the inductive effect of the ether's oxygen atom that is not present in alkane structures. To our knowledge, no kinetic parameters were reported for this pathway in the case of alkanes, likely because it is not relevant for this class of fuels. Nevertheless, Fig. 5b shows that the model predicts the formation of CH<sub>3</sub>COCH<sub>3</sub> in *n*-pentane oxidation at LT range already very well without this reaction type, indicating that this mechanism is insignificant for CH<sub>3</sub>COCH<sub>3</sub> in *n*-pentane LT oxidation. Based on the present model, CH<sub>3</sub>COCH<sub>3</sub> is produced through the LT reactions of the CH<sub>3</sub>COCH<sub>2</sub> radical that is produced by  $\beta$ -scission of the OQ1=O radical in *n*-pentane oxidation (see OQ1=O's structure in Fig. 5b).

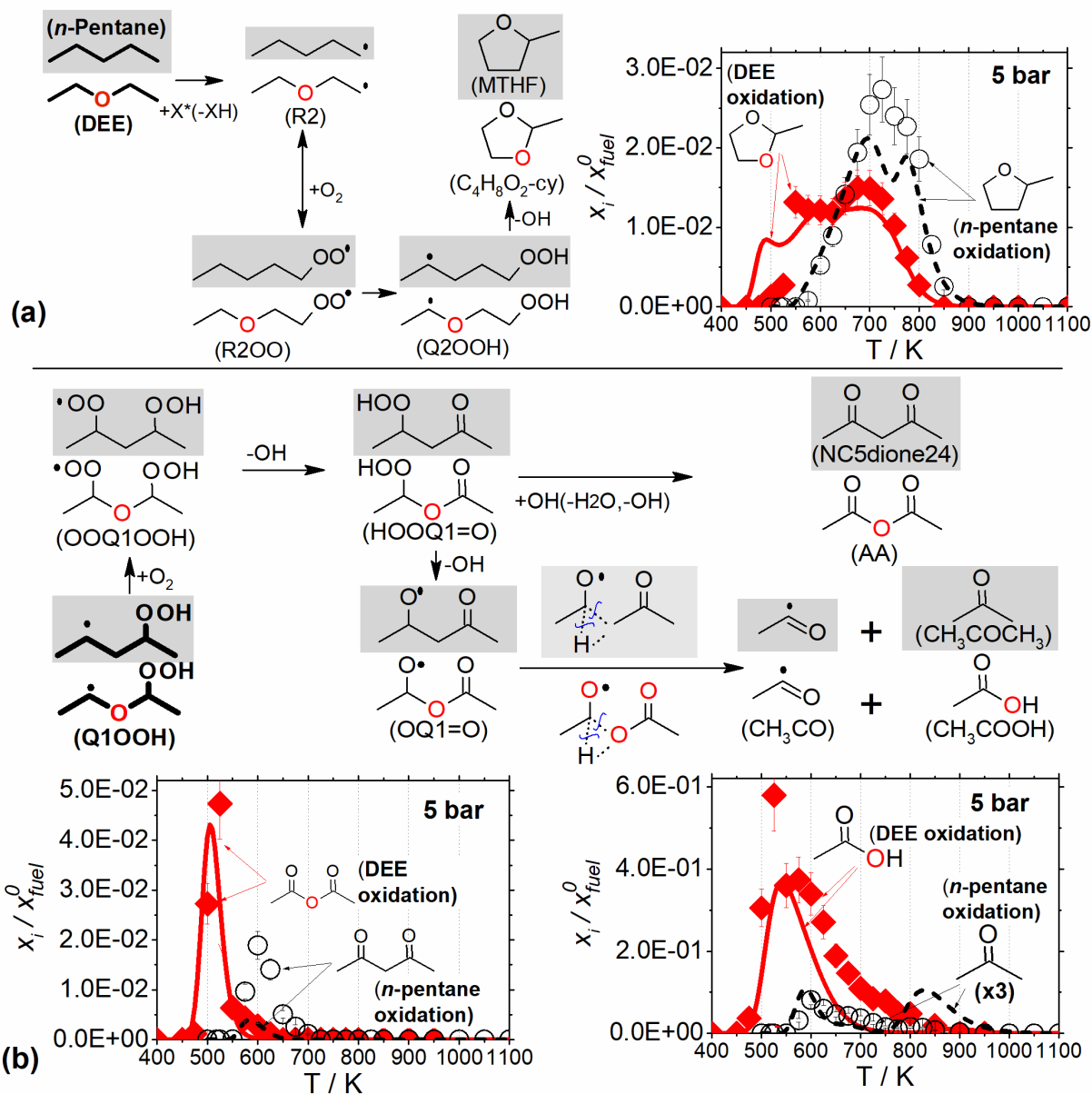


**Fig. 5.** Comparison of selected species that could have analogous formation paths from DEE and *n*-pentane (5 bar,  $\phi=1.0$ , and residence time of 2 s). **(a)** Most abundant cyclic species: *left panel*: formation diagram, *right panel*: experimental (symbols) and modeling (lines) mole fraction profiles. **(b)** Second-O<sub>2</sub>-addition products: *upper panel*: formation diagram, *lower panel*: experimental (symbols) and modeling (lines) mole fraction profiles. Formation path of Q1OOH in (b) can be seen in Fig. 4b. For clarity, a multiplication factor has been used for both experimental and modeling profiles of CH<sub>3</sub>COCH<sub>3</sub>.

### 4.3. LT oxidation of a DEE/*n*-pentane mixture

The objective of this section is to address two scientific questions, *i.e.*, how increasing the pressure influences the fuel mixture oxidation (fuel reactivity and product formation), and how DEE and *n*-pentane interact with each other in their fuel mixture.

The analyses presented before for the oxidation chemistry of neat DEE and *n*-pentane are a good starting point for studying the oxidation of their mixtures. As presented above,

pressure significantly influences the oxidation of DEE and *n*-pentane individually. In this section, the influence of pressure on a fuel mixture (DEE/*n*-pentane: 50%/50% on a molar basis) is first examined. Here the reactor was kept at 650 K, at which the largest fuel reactivity was observed (see Fig. 3a), and the pressure was increased from 2.5 bar up to 10 bar by steps of 2.5 bar. Mole fraction profiles of about 40 species were measured as a function of pressure. Figure 6a presents the experimental profiles of the two fuels (DEE, *n*-pentane), two main species (CO, CO<sub>2</sub>), and two selected primary cyclic ethers, *i.e.* MTHF (known as a fuel-specific product of *n*-pentane) and C<sub>4</sub>H<sub>8</sub>O<sub>2</sub>-cy (known as a fuel-specific product of DEE). It can be noted that these profiles change significantly at pressure lower than 5 bar, but not so much above this pressure. Such behavior is also seen for the mole fraction profiles of other species that are provided in SM3. The evolution of fuel consumption with pressure seems to be similar for DEE and *n*-pentane. Figure 6b also displays the predicted temperature dependences of the fuel consumption at different pressures up to 10 bar. Similar to the experiment, the resulting simulated profiles confirm a significant difference in reactivity between 2.5 and 5 bar, which is limited, however, when increasing the pressure further. Furthermore, *n*-pentane starts to react at temperatures as low as DEE (Fig. 6b), which differs from observations for its individual oxidation (Fig. 3a), indicating that DEE promotes *n*-pentane oxidation.

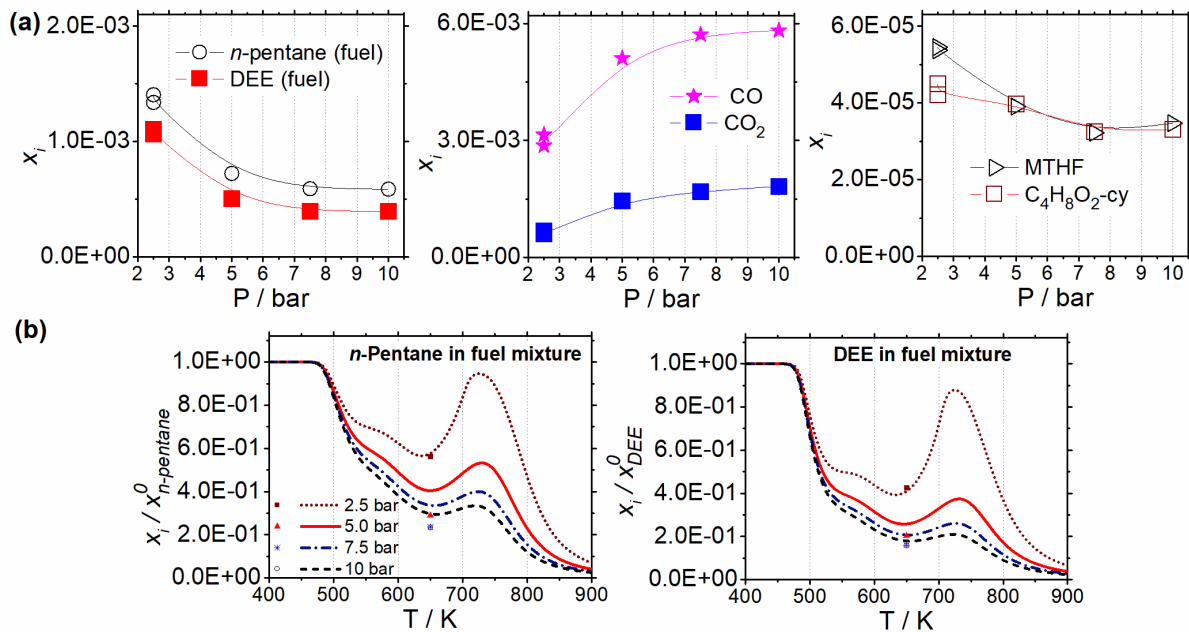


**Fig. 6. (a):** Experimental mole fractions profiles as a function of pressures for selected species measured at 650 K,  $\varphi=1.0$ , and residence time of 2 s, for the studied fuel mixture (DEE/*n*-pentane: 50%/50%). Experimental results have been connected by a spline function (thin lines) to guide the eye. **(b):** Simulated mole fraction profiles (*lines*) of fuels as a function of temperature for the fuel mixture at different pressures up to 10 bar ( $\varphi=1.0$  and residence time of 2 s) using the present model. *Symbols:* experiment, from (a) with a normalization by the inlet fuel mole fraction.

Figure 7 presents the experimental mole fractions (650 K, 5 bar) of *n*-pentane and selected LT C<sub>5</sub> intermediates measured in the fuel mixture oxidation, compared to the oxidation of neat *n*-pentane. Not unexpectedly, the reactivity of *n*-pentane increases slightly faster in the mixture than in neat *n*-pentane oxidation, and its LT oxidation products were detected in slightly higher mole fractions. This trend is consistent with simulations presented above and

with previous observations for other dual-fuel mixtures [17,41,42]. Sensitivity analyses, using the present model, for the *n*-pentane/DEE mixture (Fig. 7b) point out that several reactions of DEE promote the consumption of *n*-pentane, including the decomposition of the DEE-specific ketohydroperoxide (C2OC2KETA-1, *i.e.* HOOQ1=O in Fig. 2g), H-abstraction from DEE by OH and CH<sub>3</sub>O radicals, as well as the first and second O<sub>2</sub> additions (C<sub>2</sub>H<sub>5</sub>OC<sub>2</sub>H<sub>4</sub>-A+O<sub>2</sub>↔C<sub>5</sub>OC<sub>2</sub>H<sub>4</sub>OO-A, C<sub>2</sub>OC<sub>2</sub>-AO<sub>2</sub>H-1+O<sub>2</sub>↔C<sub>4</sub>O-AO<sub>2</sub>H-1O<sub>2</sub>).

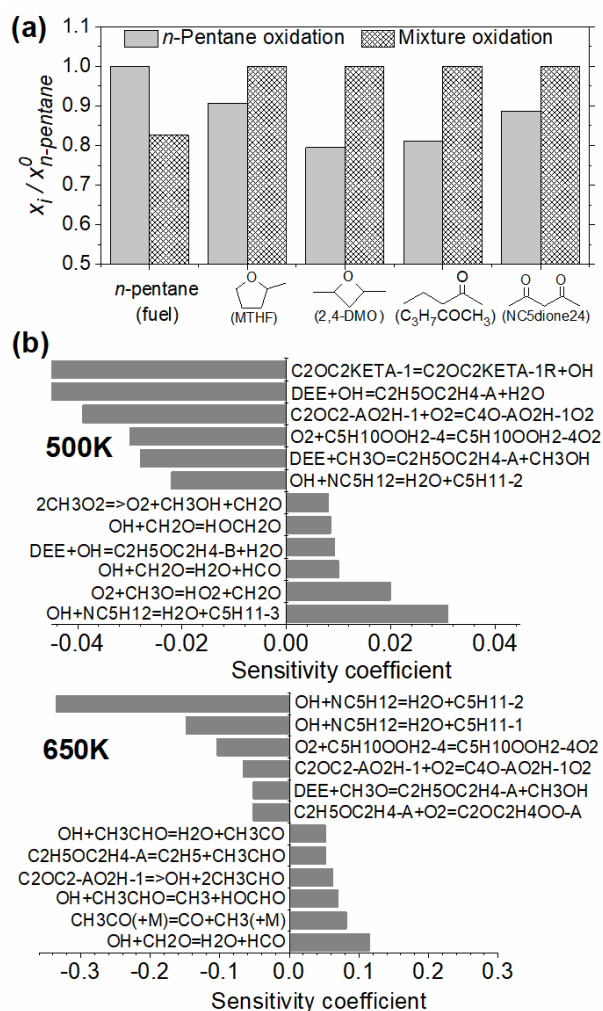


**Fig. 7.** Influence of DEE addition on the oxidation of *n*-pentane: **(a)** Experimental mole fractions of *n*-pentane and its selected fuel-specific intermediates obtained at 650 K (5 bar,  $\phi=1.0$ , and residence time of 2 s) for the oxidation of neat *n*-pentane and of the studied fuel mixture. For clarity, normalization by the highest value is performed. **(b)** Sensitivity analyses of *n*-pentane in the fuel mixture at 500 K (*top panel*) and 650 K (*bottom panel*) using the present model. Negative coefficients indicate a reaction which promotes the computed fuel consumption and vice versa. Chemical nomenclatures in (b) correspond to assignments in the CHEMKIN format kinetic mechanism.

More species were detected during the fuel mixture oxidation (about 40 species) than for *n*-pentane (about 36 species) and DEE (about 19 species) alone because the two fuels add their fuel-specific intermediates. However, in spite of the observed larger species pool, no additional, previously unidentified species were detected for the mixture by the present GC



experiments. This observation was corroborated by the PI-MBMS experiments. Examples of measured PIE curves obtained in the fuel mixture compared to those obtained for DEE and *n*-pentane individually are available in SM1 (Fig.S2).

As observed above, the reactivity of *n*-pentane is enhanced when adding DEE. It is thus interesting to examine the influence of the cross-reactions on the oxidation of the fuel mixture. Simulations with and without cross-reactions were performed, and they result in similar species profiles. Changes are seen only for a few species that are presented in Fig. S11. However, these changes are still quite limited. Sensitivity analyses for fuels were also performed, and the results pointed out that no cross-reactions of primary fuel-specific intermediates appear in sensitivity analyses of fuels (see examples in Fig. 7b for *n*-pentane), which confirms the relative insignificance of the cross-reactions in the oxidation of the fuel mixture under the studied conditions, while the fuels in the mixture influence each other through the small species pool including, *e.g.*, OH, CH<sub>3</sub>, HO<sub>2</sub>, CH<sub>3</sub>O.

## 5. Conclusions

New experimental JSR speciation data were obtained for the oxidation of DEE, *n*-pentane, and a mixture of these two fuels, at  $\phi=1$ , temperatures of 400-1100 K, and pressures of 2.5-10 bar. These elevated pressure data were compared with a dedicated kinetic model that contains the high- and low-temperature sub-mechanisms of both DEE [7] and *n*-pentane [15], with a resulting very good agreement.

Experimental and modeling results have served as a good base to comparatively analyze the oxidation of these fuels and their mixture. Influences of pressure, fuel structure, and two-component mixture oxidation *versus* that of the neat fuels were investigated with the following main results. **(i)** Compared to 1 bar, elevated pressures do not significantly affect the starting reaction temperature of DEE (~450 K), but strongly increase the global fuel reactivity and alter species formation. Elevated pressure reduces both NTC zones of DEE, with the first NTC zone almost suppressed. This reduction has been shown to mainly result from the change with pressure of the competition between the thermal decomposition reactions ( $\beta$ -scissions) and the first/second O<sub>2</sub> additions. **(ii)** Compared to *n*-pentane, DEE starts to react at much lower temperatures and it has a wider but less intense NTC behavior as well as a significant difference in LT product distribution. Some analogous reaction classes, that are very important for the LT DEE oxidation, do not seem to be significant for the case of *n*-pentane. **(iii)** DEE addition enhances, as expected, the reactivity of *n*-pentane in the fuel mixture and subsequently modifies the formation of products. The reactor pressure significantly influences the fuel reactivity and product formation when the pressure is lower than 5 bar, but this influence becomes very weak when the pressure is higher. Cross-reactions of primary fuel-specific intermediates of DEE and *n*-pentane were newly considered in the model. However, simulations demonstrate the insignificance of these cross-reactions in the oxidation of the fuel mixture under the investigated conditions. The fuels in the mixture influence each other through the small species pool including OH, CH<sub>3</sub>, HO<sub>2</sub>, CH<sub>3</sub>O, *etc.*). The fundamental study and new experimental results presented in this work about the LT chemistry of two linear five-heavy-atom fuels and their mixture at elevated pressure up to 10 bar can be considered as a solid foundation for further inspection of this chemistry in a higher-pressure range closer to practical engine operations.

## Acknowledgements

Dr. Luc-Sy Tran is grateful to the COST Action CM1404 and the Alexander von Humboldt-Foundation for financial support.

## References

- [1] K.S. Nagaprasad, N.R. Banapurmath, D. Madhu, T.M. Yunus Khan, Pre- and post-combustion emission reduction techniques for engine fuelled with diesel/DEE blends by three approaches, *Energy Sources, Part A: Recovery, Utilization and Environmental Effects*. (2019). DOI: 10.1080/15567036.2019.1663304.
- [2] D.C. Rakopoulos, C.D. Rakopoulos, E.G. Giakoumis, A.M. Dimaratos, Characteristics of performance and emissions in high-speed direct injection diesel engine fueled with diethyl ether/diesel fuel blends, *Energy*. 43 (2012) 214–224.
- [3] K. Sudheesh, J.M. Mallikarjuna, Diethyl ether as an ignition improver for biogas homogeneous charge compression ignition (HCCI) operation - An experimental investigation, *Energy*. 35 (2010) 3614–3622.
- [4] M. Mohebbi, M. Reyhanian, V. Hosseini, M.F.M. Said, A.A. Aziz, The effect of diethyl ether addition on performance and emission of a reactivity controlled compression ignition engine fueled with ethanol and diesel, *Energy Convers. Manag.* 174 (2018) 779–792.
- [5] Y. Uygun, Ignition studies of undiluted diethyl ether in a high-pressure shock tube, *Combust. Flame*. 194 (2018) 396–409.
- [6] M. Werler, L.R. Cancino, R. Schiessl, U. Maas, C. Schulz, M. Fikri, Ignition delay times of diethyl ether measured in a high-pressure shock tube and a rapid compression machine, *Proc. Combust. Inst.* 35 (2015) 259–266.
- [7] L.-S. Tran, O. Herbinet, Y. Li, J. Wullenkord, M. Zeng, E. Bräuer, F. Qi, K. Kohse-Höinghaus, F. Battin-Leclerc, Low-temperature gas-phase oxidation of diethyl ether: Fuel reactivity and fuel-specific products, *Proc. Combust. Inst.* 37 (2019) 511–519.
- [8] Z. Serinyel, M. Lailliau, S. Thion, G. Dayma, P. Dagaut, An experimental chemical kinetic study of the oxidation of diethyl ether in a jet-stirred reactor and comprehensive modeling, *Combust. Flame*. 193 (2018) 453–462.
- [9] K.C. Salooja, Mechanism of combustion of diethyl ether. Comparative studies of diethyl ether, pentane and acetaldehyde, *Combust. Flame*. 9 (1965) 33–41.
- [10] Y. Sakai, J. Herzler, M. Werler, C. Schulz, M. Fikri, A quantum chemical and kinetics modeling study on the autoignition mechanism of diethyl ether, *Proc. Combust. Inst.* 36 (2017) 195–202.
- [11] E. Hu, Y. Chen, Z. Zhang, J.-Y. Chen, Z. Huang, Ab initio calculation and kinetic modeling study of diethyl ether ignition with application toward a skeletal mechanism for CI engine modeling, *Fuel*. 209 (2017) 509–520.
- [12] Z. Tang, L. Zhang, X. Chen, G. Tang, Improved kinetic mechanism for diethyl ether oxidation with a reduced model, *Energy Fuels*. 31 (2017) 2803–2813.
- [13] J. Eble, J. Kiecherer, M. Olzmann, Low-temperature autoignition of diethyl ether/O<sub>2</sub> mixtures: Mechanistic considerations and kinetic modeling, *Z. Phys. Chem.* 231 (2017) 1603–1623.
- [14] H.J. Curran, Developing detailed chemical kinetic mechanisms for fuel combustion, *Proc. Combust. Inst.* 37 (2019) 57–81.
- [15] J. Bugler, A. Rodriguez, O. Herbinet, F. Battin-Leclerc, C. Togbe, G. Dayma, P. Dagaut, H.J. Curran, An experimental and modelling study of n-pentane oxidation in two jet-stirred

- reactors: The importance of pressure-dependent kinetics and new reaction pathways, *Proc. Combust. Inst.* 36 (2017) 441–448.
- [16] A. Rodriguez, O. Herbinet, Z. Wang, F. Qi, C. Fittschen, P.R. Westmoreland, F. Battin-Leclerc, Measuring hydroperoxide chain-branching agents during n-pentane low-temperature oxidation, *Proc. Combust. Inst.* 36 (2017) 333–342.
- [17] H. Jin, J. Pieper, C. Hemken, E. Bräuer, L. Ruwe, K. Kohse-Höinghaus, Chemical interaction of dual-fuel mixtures in low-temperature oxidation, comparing n-pentane/dimethyl ether and n-pentane/ethanol, *Combust. Flame.* 193 (2018) 36–53.
- [18] R. Minetti, A. Roubaud, E. Therssen, M. Ribaucour, L.R. Sochet, The chemistry of pre-ignition of n-pentane and 1-pentene, *Combust. Flame.* 118 (1999) 213–220.
- [19] C.K. Westbrook, H.J. Curran, W.J. Pitz, J.F. Griffiths, C. Mohamed, S.K. Wo, The effects of pressure, temperature, and concentration on the reactivity of alkanes: Experiments and modeling in a rapid compression machine, *Proc. Combust. Inst.* 27 (1998) 371–378.
- [20] J.F. Griffiths, P.A. Halford-Maw, D.J. Rose, Fundamental features of hydrocarbon autoignition in a rapid compression machine, *Combust. Flame.* 95 (1993) 291–306.
- [21] H. Zhao, A.G. Dana, Z. Zhang, W.H. Green, Y. Ju, Experimental and modeling study of the mutual oxidation of N-pentane and nitrogen dioxide at low and high temperatures in a jet stirred reactor, *Energy.* 165 (2018) 727–738.
- [22] J. Bourgalais, Z. Goud, O. Herbinet, G.A. Garcia, P. Arnoux, Z. Wang, L.-S. Tran, G. Vanhove, M. Hochlaf, L. Nahon, F. Battin-Leclerc, Isomer-sensitive characterization of low temperature oxidation reaction products by coupling a jet-stirred reactor to an electron/ion coincidence spectrometer: case of n-pentane, *Phys. Chem. Chem. Phys.* 22 (2019) 1222–1241.
- [23] C. Bai, N. Liu, B. Zhang, Experimental investigation on the lower flammability limits of diethyl ether/n-pentane/epoxypropane-air mixtures, *J Loss Prevent Proc.* 57 (2019) 273–279.
- [24] O. Herbinet, B. Husson, H. Le Gall, F. Battin-Leclerc, Comparison study of the gas-phase oxidation of alkylbenzenes and alkylcyclohexanes, *Chem. Eng. Sci.* 131 (2015) 49–62.
- [25] L.-S. Tran, M. Verdicchio, F. Monge, R.C. Martin, R. Bounaceur, B. Sirjean, P.-A. Glaude, M.U. Alzueta, F. Battin-Leclerc, An experimental and modeling study of the combustion of tetrahydrofuran, *Combust. Flame.* 162 (2015) 1899–1918.
- [26] Z. Zhou, X. Du, J. Yang, Y. Wang, C. Li, S. Wei, L. Du, Y. Li, F. Qi, Q. Wang, The vacuum ultraviolet beamline/endstations at NSRL dedicated to combustion research, *J Synchrotron Rad.* 23 (2016) 1035–1045.
- [27] L.-S. Tran, J. Pieper, H.-H. Carstensen, H. Zhao, I. Graf, Y. Ju, F. Qi, K. Kohse-Höinghaus, Experimental and kinetic modeling study of diethyl ether flames, *Proc. Combust. Inst.* 36 (2017) 1165–1173.
- [28] F. Gillespie, W.K. Metcalfe, P. Dirrenberger, O. Herbinet, P.-A. Glaude, F. Battin-Leclerc, H.J. Curran, Measurements of flat-flame velocities of diethyl ether in air, *Energy.* 43 (2012) 140–145.
- [29] Z. Zhang, E. Hu, C. Peng, Z. Huang, Experimental and kinetic study on ignition delay times of diethyl ether, *SAE Int J Fuels Lubr.* 8 (2015) 111–118.
- [30] Y. Di, Z. Huang, N. Zhang, B. Zheng, X. Wu, Z. Zhang, Measurement of laminar burning velocities and markstein lengths for diethyl ether - Air mixtures at different initial pressure and temperature, *Energy Fuels.* 23 (2009) 2490–2497..

- [31] K. Yasunaga, F. Gillespie, J.M. Simmie, H.J. Curran, Y. Kuraguchi, H. Hoshikawa, M. Yamane, Y. Hidaka, A Multiple Shock Tube and Chemical Kinetic Modeling Study of Diethyl Ether Pyrolysis and Oxidation, *J. Phys. Chem. A*. 114 (2010) 9098–9109.
- [32] N. Vin, O. Herbinet, F. Battin-Leclerc, Diethyl ether pyrolysis study in a jet-stirred reactor, *J. Anal. Appl. Pyrolysis*. 121 (2016) 173–176.
- [33] J. Hashimoto, K. Tanoue, N. Taide, Y. Nouno, Extinction limits and flame structures of 1-butanol and Diethyl Ether non-premixed flames, *Proc. Combust. Inst.* 35 (2015) 973–980.
- [34] J. Bugler, B. Marks, O. Mathieu, R. Archuleta, A. Camou, C. Grégoire, K.A. Heufer, E.L. Petersen, H.J. Curran, An ignition delay time and chemical kinetic modeling study of the pentane isomers, *Combust. Flame*. 163 (2016) 138–156.
- [35] J. Bugler, K.P. Somers, E.J. Silke, H.J. Curran, Revisiting the kinetics and thermodynamics of the low-temperature oxidation pathways of alkanes: A case study of the three pentane isomers, *J. Phys. Chem. A*. 119 (2015) 7510–7527.
- [36] V.P. Zhukov, V.A. Sechenov, A.Yu. Starikovskii, Self-ignition of a lean mixture of n-pentane and air over a wide range of pressures, *Combust. Flame*. 140 (2005) 196–203.
- [37] M.A. Oehlschlaeger, D.F. Davidson, J.T. Herbon, R.K. Hanson, Shock tube measurements of branched alkane ignition times and OH concentration time histories, *Int. J. Chem. Kinet.* 36 (2004) 67–78.
- [38] A.P. Kelley, A.J. Smallbone, D.L. Zhu, C.K. Law, Laminar flame speeds of C5 to C8 n-alkanes at elevated pressures: Experimental determination, fuel similarity, and stretch sensitivity, *Proc. Combust. Inst.* 33 (2011) 963–970.
- [39] C.W. Gao, J.W. Allen, W.H. Green, R.H. West, Reaction Mechanism Generator: Automatic construction of chemical kinetic mechanisms, *Comput. Phys. Commun.* 203 (2016) 212–225.
- [40] Z. Wang, X. Zhang, L. Xing, L. Zhang, F. Herrmann, K. Moshhammer, F. Qi, K. Kohse-Hoeinghaus, Experimental and kinetic modeling study of the low- and intermediate-temperature oxidation of dimethyl ether, *Combust. Flame*. 162 (2015) 1113–1125.
- [41] D. Kaczmarek, B. Atakan, T. Kasper, Investigation of the partial oxidation of methane/n-heptane-mixtures and the interaction of methane and n-heptane under ultra-rich conditions, *Combust. Flame*. 205 (2019) 345–357.
- [42] Z. Lu, Y. Yang, M.J. Brear, Oxidation of PRFs and ethanol/iso-octane mixtures in a flow reactor and the implication for their octane blending, *Proc. Combust. Inst.* 37 (2019) 649–656.